J. Fluid Mech. (1991), vol. 223, pp. 165–191
Printed in Great Britain

Effects of rotation on turbulent mixing across a density interface

By M. FLEURY†, M. MORY, E. J. HOPFINGER AND D. AUCHERE

Institut de Mécanique de Grenoble, Domaine Universitaire, BP 53X, 38041 Grenoble Cédex, France

(Received 2 September 1989 and in revised form 2 July 1990)

The effect of rotation on mixing across a density interface is studied experimentally in a two-layer stratified fluid. Mixing is caused by turbulence produced in one of the layers by an oscillating grid. The flow depends on the Richardson number $Ri = g'l/u^2$ and the Rossby number $Ro = u/2\Omega l$. The most important result is the observed decrease of the entrainment rate E in the presence of rotation, when compared with non-rotating experiments. In a certain range of the two parameters, a general entrainment law in the form $E = 0.5RoRi^{-1}$ is established, whereas the entrainment law in non-rotating conditions is $E = 1.6Ri^{-\frac{3}{2}}$. Additional information concerning the dynamics of the interface in rotating conditions is provided by interface displacement spectra, showing that rotation favours low-frequency oscillations of the interface, whereas high-frequency oscillations are not modified by rotation. Finally, the role of inertial waves is discussed on the basis of velocity measurements in the non-stirred layer.

1. Introduction

For many geophysical flows, and in particular for the ocean, determining the dynamics of density interfaces is one of the crucial stages in modelling general circulation. The dynamics of thermoclines is subject to two major unknown factors. First, there is the question of mixing; thermoclines move in time, owing to entrainment of fluid across them. It is important to predict entrainment and, consequently, the exchanges between kinetic energy and potential energy. The other question concerns energy transmission across interfaces. Numerous studies of thermocline dynamics have focused on mixing. In geophysical fluids mixing may result either from Kelvin–Helmholtz instabilities of the current mean shear across the interface, or from turbulent motions coming from the mixed layer. This paper considers the effect of turbulence without mean shear. In the laboratory such a turbulent field can be produced by an oscillating grid. Since, for most cases of interest, the Richardson number $Ri = g'l/u^2$ is high (l is the integral lengthscale, u the r.m.s. horizontal turbulent velocity and $g' = \Delta\rho g/\rho$ the reduced gravity), turbulent mixing across a density interface is considered to be a small-scale phenomenon compared to the integral lengthscale of turbulent motions. The first studies on the subject (Turner 1973; Thompson & Turner 1975; Hopfinger & Toly 1976; Linden 1973; Long 1978; Fernando & Long 1985; E & Hopfinger 1986, among others) did not consider the effect of background rotation on mixing. However, in

† Present address: Chesapeake Bay Institute, The Rotunda, 711W, 40th Street, Baltimore, Md 21211, USA.

oceanic situations, the effect of rotation may not always be negligible. The depths of the benthic layer or of the mixed layer at the ocean surface may be of the order of magnitude of the turbulent Ekman layer, with a turbulent Rossby number of the order of 1. Experiments on the effects of rotation on turbulent entrainment at Rossby numbers of this order, using an oscillating grid in a tank subjected to mean rotation, were recently reported by Maxworthy (1986) and Noh & Long (1987). A significant decrease in entrainment rate was observed by these authors. In addition, energy transmission across the interface is enhanced by rotation. Maxworthy speculated that the transport of energy by inertial waves reduces the amount of kinetic energy available at the interface for mixing, and is therefore responsible for the decrease in entrainment rates.

This paper presents the results of an experimental study aimed at determining non-dimensional entrainment laws for mixing in a rotating system. In a non-rotating fluid, various authors (Turner 1973; E & Hopfinger 1986) obtained a variation of entrainment rate E in the form

$$E = \frac{u_e}{u} = KRi^{-\frac{3}{2}} = K\left(\frac{g'l}{u^2}\right)^{-\frac{3}{2}} \tag{1}$$

(u_e is the entrainment velocity, i.e. the velocity of the mean displacement of the interface). In a rotating system, the entrainment rate depends on both the Richardson number and the Rossby number $Ro = u/2\Omega l$, Ω being the rotation rate of the system.

This paper contains six main parts. Sections 2 and 3 are devoted to a description of the experimental set-up and measurement techniques. A new apparatus was built in our laboratory, which records the instantaneous position of the interface using the propagation of ultrasonic waves (see §3). Qualitative observations are described in §4. Entrainment rate measurements are shown in §5; these confirm the earlier observations that rotation decreases the entrainment rate. A general entrainment law is established:

$$E = 0.5RoRi^{-1}. \tag{2}$$

In order to identify more clearly the effect of rotation on the dynamics of interface oscillations, the instantaneous displacements of the interface were also recorded and analysed by computing frequency interface displacement spectra. This study was suggested by the recent work by Hannoun, Fernando & List (1988) and Hannoun & List (1988) (for grid turbulence without rotation), which provided new insights into the mixing process. Interface displacement spectra are called 'internal wave spectra' in Hannoun & List's paper. Both terminologies actually designate the same quantity. 'Interface displacement spectra' is preferred here as it is not clear whether the spectra measured represent only internal wave motions. The interface displacement spectra obtained by the present authors in a system subjected to rotation are presented in §6. Finally, §7 contains measurements of velocities in the layer that is not stirred by grid oscillation. These measurements give a quantitative estimate of energy transmission across the interface by inertial waves.

2. Experimental methods

2.1. *Installation*

The installation used by Hopfinger, Browand & Gagne (1982) to study rotationally dominated grid turbulence was modified to produce a two-layer stratified fluid. The tank, shown schematically in figure 1, is transparent and cylindrical, 40 cm in

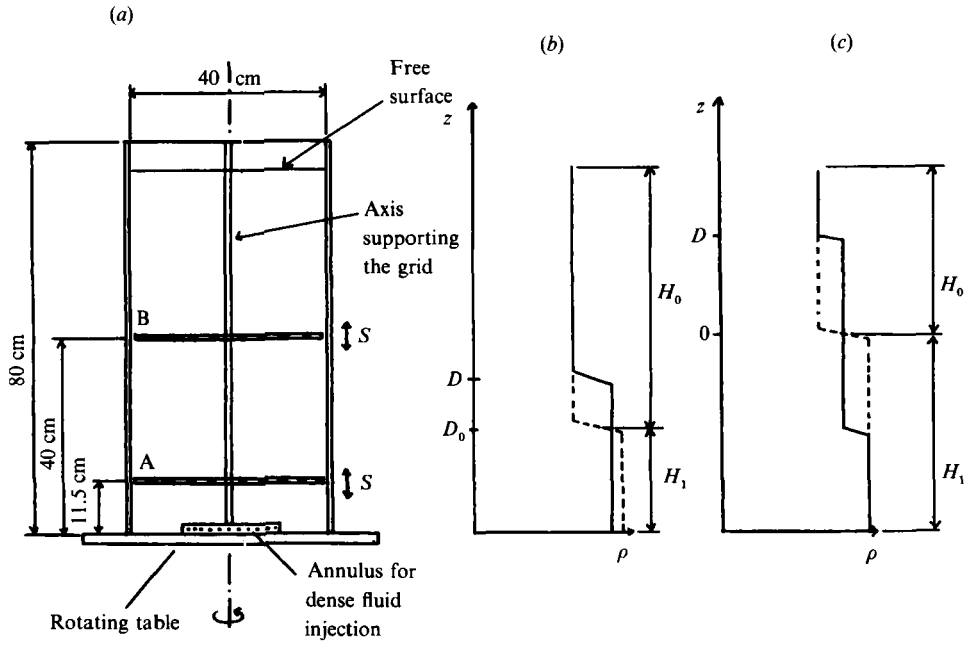

FIGURE 1. Schematic diagram of experimental conditions: (*a*) experimental apparatus, also indicating the grid locations A and B; (*b*) density profile when the grid is at position A; (*c*) density profile when the grid is at position B. (Dashed lines mark the initial density profiles. Solid lines give a typical density profile during an experiment.)

diameter and 80 cm in depth. It is fixed on a rotating table whose rotation rate Ω can be adjusted continuously up to 2π rad s^{-1} with better than 1% accuracy. The two-layer stratification is prepared while the tank is rotating. Rotation of the tank was started after it was filled with fresh water up to depth H_0. Salty water was then slowly introduced through holes in an annulus fixed at the bottom of the tank, until the dense fluid layer reached depth H_1. Owing to rotation, the interface takes a parabolic form. The highest rotation rate used in our experiment ($\Omega = \pi$ rad s^{-1}) produces a maximum vertical displacement of the interface of less than 2 cm at the perimeter of the cylinder. The slope of the interface is therefore weak. The subsequent variation of the properties of turbulence at the interface (turbulence level and lengthscale) from the centre of the tank to its perimeter are taken into account: most measurements are local (see §3), and all quantities are estimated at the measured position of the interface.

Turbulence is generated by an oscillating grid when both layers are in solid-body rotation. As in Hopfinger *et al.*'s experiments the grid was made of 1 cm square bars with a mesh $M = 5$ cm. The grid was oscillated about a horizontal plane. Two cases were investigated. In the first configuration (denoted A, figure 1) the mean position of the grid is 11.5 cm above the bottom of the tank. The initial position of the density interface is 25 cm above the grid midplane. In this configuration, the interface displacement can be observed over a very long period of time, but the density difference between the two layers $\Delta\rho$ varies as the interface moves up. In the second configuration (denoted B, figure 1) the mean position of the grid is in the middle of the tank and the initial position of the density interface coincides with the grid midplane. When the grid starts to oscillate, the mean stratification profile evolves rapidly into a three-layer stratified fluid, with the two interfaces moving

symmetrically with respect to the grid midplane. The advantage of this configuration lies in the constancy of the density difference across the interfaces (half the initial density difference). However, the distance over which the interface displacement can be observed is reduced by a factor of two compared with configuration A. This was a major restriction for studying entrainment in the domain of the tank where turbulence is quasi-two-dimensional. For this reason, entrainment rates were measured in configuration A when the Rossby number $Ro < 0.2$, and in configuration B when $Ro > 0.2$. Grid oscillation conditions are determined by the stroke S (twice the amplitude) and the frequency n. Two couples (S, n) were used in our experiments, namely (4 cm, 6.6 Hz) and (3 cm, 6 Hz).

2.2. *The structure of turbulence*

Experiments by McDougall (1979) showed that r.m.s. turbulent velocity components produced by an oscillating grid are not modified by the stratification except in a region including the interface whose thickness is about one integral lengthscale. Measurements of characteristic turbulent velocities and lengthscales, performed by Hopfinger, Griffiths & Mory (1983) and by Mory & Hopfinger (1985) in the same rotating apparatus (but in homogeneous fluid) therefore provide the consistent estimates for these quantities needed for the determination of the Richardson and Rossby numbers in the vicinity of the interface. With rotation, turbulence becomes non-isotropic: in particular, the integral lengthscale along the direction parallel to the rotation axis is significantly larger than the integral lengthscale in a direction perpendicular to this axis. A more complete description of the effect of rotation on the structure of turbulence can be found in the papers referred to above. Hopfinger *et al.* (1983) only measured the turbulent velocity component $u(z)$ in a plane perpendicular to the axis of rotation and the integral lengthscale $l(z)$ also in a direction perpendicular to this axis. These measurements are used to present our results in non-dimensional form. However, we had the opportunity during the course of the present study to measure the turbulent velocity component w parallel to the rotation axis. These results are presented in the Appendix, because it is useful to have an idea of the anisotropy of turbulence subjected to rotation.

Three cases were considered, depending on whether the distance $D(t)$ of the interface from the grid midplane is smaller than a typical distance Z_T, greater than a typical distance Z_R or in the range $Z_T < D(t) < Z_R$.

(i) If $D(t) < Z_T$, the effect of rotation is negligible and $u(z)$ and $l(z)$ vary as obtained by Hopfinger & Toly (1976) in non-rotating oscillating grid turbulence for $z < D(t)$:

$$u(z) = K_1 \frac{S^{\frac{3}{2}} M^{\frac{1}{2}} n}{z}, \tag{3}$$

$$l(z) = K_2 z. \tag{4}$$

K_1 and K_2 are constants. The local Rossby number $Ro(z) = u(z)/2\Omega l(z)$ decreases with increasing distance from the grid.

(ii) If $Z_T < D(t) < Z_R$, under the effect of rotation the decay of $u(z)$ with z $(Z_T < z < D(t))$ slows down suddenly and the increase of $l(z)$ with z is much slower.

(iii) If $D(t) > Z_R$, $u(z)$ and $l(z)$ are quasi-independent of z for $D(t) > z > Z_R$, turbulent velocity profiles and turbulent kinetic energy spectra have shown (Hopfinger *et al.* 1983; Mory & Hopfinger 1986) that the turbulence is quasi-two-dimensional in this upper part of the tank. From the data obtained by Hopfinger *et al.* (1983) and Mory & Hopfinger (1985) we estimate that the velocity and the

integral lengthscale in this part of the tank ($D(t) > Z_R$) can be related to the corresponding values at the transition $z = Z_T$ as follows:

$$u(z > Z_R) \approx 0.55u(Z_T) \approx 1.7 \text{ cm s}^{-1}, \tag{5}$$

$$l(z > Z_R) \approx l(Z_T)/0.55 \approx 2.5 \text{ cm}. \tag{6}$$

We verified that $u(Z_R)\,l(Z_R) \approx u(Z_T)\,l(Z_T)$, implying that the Reynolds number is approximately the same at the two positions in the tank. This is not a surprising result since this property is verified in the part of the tank closest to the grid ($l(z) \propto z$ and $u(z) \propto z^{-1}$ for $z < Z_T$) and the decay is reduced by rotation in the domain $z > Z_T$.

Entrainment rates (§5) were measured either when $D(t) < Z_T$ or when $D(t) > Z_R$.

The value of the constant K_1 in (3) is about 0.26. The value of the constant K_2 serving to determine the integral lengthscale (4) is usually in the range 0.10–0.25. Hopfinger & Toly (1976) obtained $K_2 = 0.25$ in a similar experiment. Using this value, Hopfinger *et al.* (1983) estimated that the Rossby number $Ro(Z_T) = 0.2$ at this transition. More recent measurements (Mory & Hopfinger 1985) of the integral lengthscale have shown that a better fit is obtained in our experiment (with $S =$ 4 cm) when $K_2 = 0.14$. In the following we take $K_2 = 0.14$ to estimate the Richardson and Rossby numbers for the grid oscillation conditions ($S = 4$ cm, $n = 6.6$ Hz) and $K_2 = 0.25$ for the conditions ($S = 3$ cm, $n = 6$ Hz). This choice has little objective justification, but it will make the entrainment rate data for the two conditions collapse on the same curve (§5). It will therefore be easier to identify the dependence of entrainment rates on the Richardson and Rossby numbers.

2.3. *Visualization techniques*

Three different visualization techniques were used in the course of this study: shadowgraphs, a fluorescent dye technique and particle streaks.

Shadowgraph pictures provided important qualitative details of the density field (see §4). We also analysed movies of shadowgraphs to estimate the entrainment rates under certain conditions (see §5.2). The shadowgraph technique is a classic one, which need not be described here. It is however necessary to mention that the parallel light beam is deflected by the round surface of the cylindrical tank, which acts as a focusing lens. While the interpretation of horizontal distances is therefore altered, and the shadowgraph only gives a clear view of the density field in the central part of the tank, this disadvantage turns out to be an advantage when the mean position of the interface is determined: the light beam passing through the outer part of the tank focuses to such an extent that the parts of the shadowgraph on the left and right sides of each picture correspond to a density field integrated over a large part of the tank. This helps to determine the mean position of the interface.

Visualizations of the interface were also obtained by a vertical sheet of light 1 cm thick passing through the axis of the tank. For these visualizations the dense salty water was initially coloured by fluoresceine dye. Instantaneous photographs revealed details of the interface structure (see §4).

Finally, we measured the velocities in the non-mixed layer using photographs of particle displacements over a period of time of 0.5 s (see §7). The motions are visualized by a horizontal sheet of light about 3.5 cm thick. The camera is placed above the tank and pictures were taken through the upper transparent cover. The particles used (0.33 mm in diameter) were polystyrene beads and were used after adjustment of their density.

3. Measurement of the interface displacement by an ultrasonic probe

3.1. *Physical principle*

A new system has been developed at the Institut de Mécanique de Grenoble. Interface displacements are deduced from measuring the travelling time of an ultrasonic wave packet between the transceiver and a reflector placed on its path in the salty water (figure 2). Because the speed of sound is proportional to the salinity, the travelling time decreases as the total quantity of salt in the wave path increases or, equivalently, as the interface height increases.

The time taken by the wave to travel from the transceiver to the reflector and back is

$$\theta = 2\int_0^{Z_p} \frac{1}{c(z,t)}\,dz, \tag{7}$$

where $c(z,t)$ is the local value of the speed of sound, z is a vertical axis with its origin on the reflector, t is the time and Z_p designates the position of the transceiver. The speed $c(z,t)$ is (Bank 1966):

$$c(z,t) = c_p + aS(z,t) + bT(z,t), \tag{8}$$

where $S(z,t)$ and $T(z,t)$ are local values of salinity and temperature, $c_p \approx 1473$ m s^{-1} is the sound wave speed in pure water at 20° C and $a \approx 1.10$ m s^{-1} ppm^{-1}, $b \approx 3.54$ m s^{-1} °C^{-1}. Thus

$$\theta = 2\frac{Z_p}{c_p} - \frac{2a}{c_p^2}\int_0^{Z_p} S(z,t)\,dz - \frac{2b}{c_p^2}\int_0^{Z_p} T(z,t)\,dz, \tag{9}$$

with a negligible error of the order of

$$\int_0^{Z_p} [aS(z,t) + bT(z,t)]^2/c_p^3\,dz.$$

Because θ is measured with an unknown but constant offset, the difference

$$\Delta\theta = \theta - \theta_0 = -\frac{2a}{c_p^2}\int_0^{Z_p} (S(z,t) - S_0)\,dz - \frac{2b}{c_p^2}\int_0^{Z_p} (T(z,t) - T_0)\,dz \tag{10}$$

is studied instead. θ_0 is a reference time at which T_0 and S_0 are known. A linear relationship between the position D of the middle of the interfacial layer and the time difference $\Delta\theta$ can be obtained by considering a piecewise linear salinity profile:

$$\left.\begin{aligned} &S(z,t) = 0 && \text{for} \quad z > D + \tfrac{1}{2}e, \\ &S(z,t) = S && \text{for} \quad z < D - \tfrac{1}{2}e, \\ &S(z,t) = S(D + \tfrac{1}{2}e - z)/e && \text{for} \quad D - \tfrac{1}{2}e < z < D + \tfrac{1}{2}e; \end{aligned}\right\} \tag{11}$$

e is the interface thickness. The use of such a profile is justified by the conductivity recordings by E & Hopfinger (1986) among others. The only crucial point is that the density is uniform in both layers except inside the interfacial layer. In any case what is measured is the position of the mean salinity on the path between the transceiver and the reflector. For the piecewise salinity profile chosen, this position corresponds to the position D of the middle of the interfacial layer. Introducing (11) in (10) and assuming $T(z,t) = T_0 = \text{const.}$ gives

$$\Delta\theta = -\frac{2a}{c_p^2}(SD - S_0 D_0). \tag{12}$$

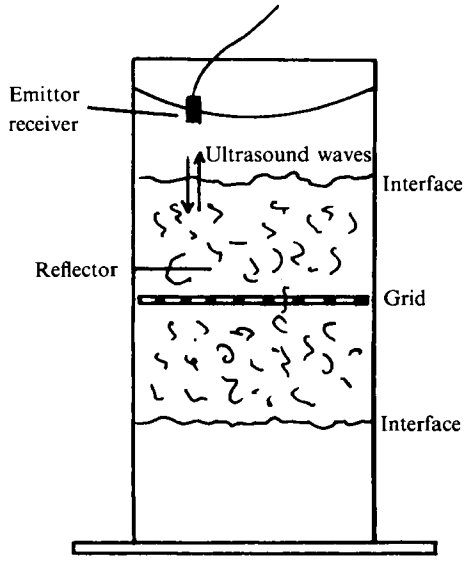

FIGURE 2. Schematic diagram of the ultrasonic system for the measurement of density interface displacements.

It is worth noting that $\Delta\theta$ does not depend on the interface thickness e. In configuration B, the mean salinity S is constant in time throughout an experiment ($S = S_0$) and $\Delta\theta$ is therefore a linear function of the interface displacement

$$\Delta\theta = -\frac{2aS}{c_p^2}(D - D_0). \tag{13}$$

Calibration gives a typical value $2aS/c_p^2 \approx 1.3\ 10^{-5}$ s m^{-1}. Thus a displacement of 1 mm produces a variation in the travelling time of the wave packet of 13 ns.

3.2. *Calibration and resolution*

For each experiment the constant $2aS/c_p^2$ is determined (c_p depends on temperature). The time θ_0, also used as the reference time in (10), is measured at the beginning of the experiment when the interface is below the reflector. At the end of the experiment, a second time θ_1 is measured after the interface has reached the probe. The value $2aS/c_p^2$ is therefore equal to $(\theta_0 - \theta_1)/Z_p$, Z_p being the distance between the transceiver and the reflector. The accuracy of this method is greater than 2% of the value of $2aS/c_p^2$. As mentioned before, we assume that the temperature is uniform and constant. Actually, temperature variations are less than 0.1 °C over half an hour, which is the typical duration of an experiment. The subsequent error in $\Delta\theta$ (see (10)) is about 100 ns, i.e. 5% of the total variation of travelling time due to mixing ($c_p \approx 1500$ m s^{-1}, $Z_p \approx 15$ cm and $b \approx 4$ m s^{-1} °C^{-1} are adopted for this estimate).

The time resolution of the apparatus determines the smallest interface displacement that can be measured by the system. The frequency of the wave (2×10^6 Hz) and the characteristics of the AD converter gives a minimum variation of about 2 ns in the travelling time of the wave that can be measured. The smallest displacement of the position of the middle of the interfacial layer measured by the apparatus is therefore 0.15 mm (with $2aS/c_p^2 \approx 1.3\ 10^{-5}$ s m^{-1}). This 'vertical resolution' does not mean that the vertical distribution of density is determined. The apparatus measures the total amount of salt integrated over the vertical direction.

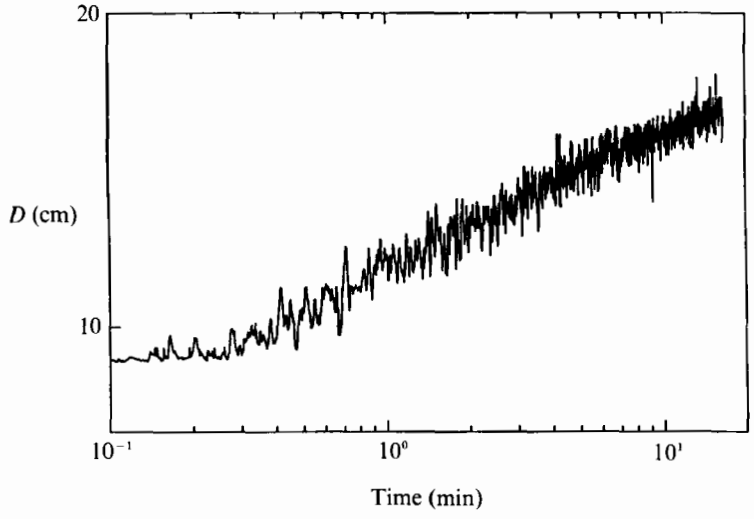

FIGURE 3. Recording of instantaneous interface displacements as a function of time during a typical experiment ($\Delta\rho/\rho = 1.15\,\%$, $S = 3$ cm, $n = 6$ Hz, $\Omega = 0.3\pi$ rad s^{-1}).

This quantity is related to the instantaneous local interface position, but the thickness of the interfacial layer is not determined.

The transceiver is a piezoelectric oscillator of surface area 8 mm × 8 mm and the reflector is a cylindrical stem of diameter 1 mm. The typical size of 8 mm determines the smallest lengthscale of deformation of the interface in the horizontal direction that can be captured by the apparatus. The signal delivered by the apparatus corresponds to the position, as a function of time, of the middle of the interfacial layer averaged over an horizontal surface of extent 8 mm × 8 mm. Using a model of internal waves we show in §6 that the smallest wavelength $\lambda_c \approx 8$ mm imposes a low-pass cutoff frequency in the measurement in time of interface displacements. This frequency cutoff is quite restrictive as the lengthscale λ_c is rather large. We shall see however that our set-up is able to capture significant characteristics of the dynamics of the interface.

3.3. *Data processing*

Figure 3 shows the variation in the position of the middle of the interface D as a function of time for a typical experiment. The origin of D is at the grid midplane and time is taken from the start of grid oscillation. We determine the entrainment velocity $u_e = \mathrm{d}D/\mathrm{d}t$ by fitting the data with a power law of the form

$$D(t) = Ct^a. \tag{14}$$

Agreement with a power law is best shown when the data are low-pass filtered at 0.2 Hz (figure 4). The entrainment velocity is then

$$u_e = \frac{\mathrm{d}D}{\mathrm{d}t} = Cat^{a-1} = C^{1/a}aD^{(a-1)/a}. \tag{15}$$

Instantaneous fluctuations of the interface were also studied after subtracting the entrainment contribution as estimated by (14) (see figure 5). Frequency spectra were computed from these signals using fast Fourier transforms over periods of time of 227 s (4096 points) and then averaged for successive records (up to 20 minute records are analysed).

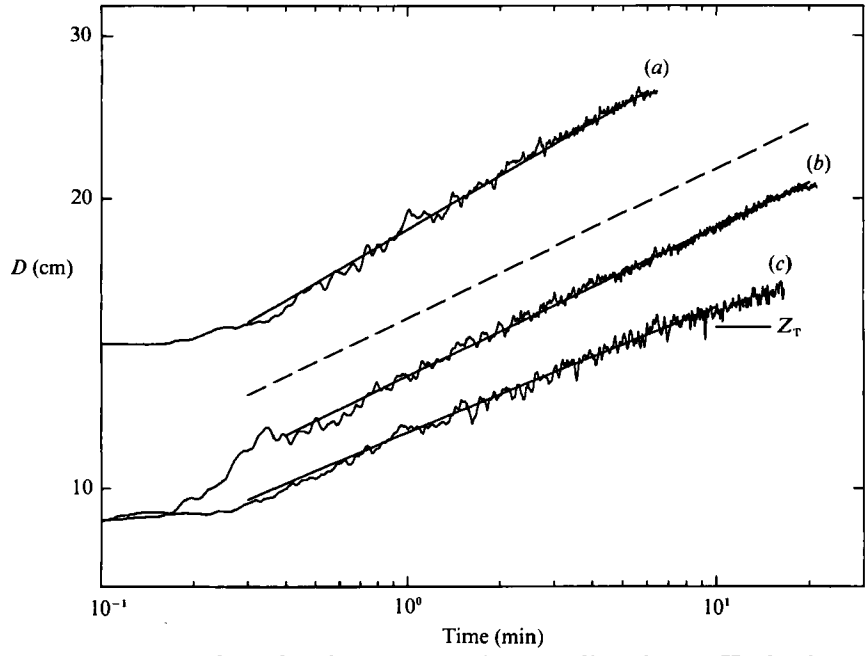

FIGURE 4. Recordings of interface displacements, low-pass filtered at 0.2 Hz, for three experiments: (*a*) no rotation, $S = 4$ cm, $n = 6.6$ Hz, $\Delta\rho/\rho = 1.30\%$; (*b*) no rotation, $S = 3$ cm, $n = 6$ Hz, $\Delta\rho/\rho = 0.90\%$; (*c*) rotation, $\Omega = 0.3\pi$ rad s^{-1}, $S = 3$ cm, $n = 6$ Hz, $\Delta\rho/\rho = 1.15\%$. The position Z_T of the transition in turbulent structure is indicated on this curve. Straight lines superimposed on the data show the fit to a power law of the form $D(t) = Ct^a$. The dashed straight line shows the slope of the power law associated with an entrainment law in the form $E \propto Ri^{-\frac{3}{2}}$.

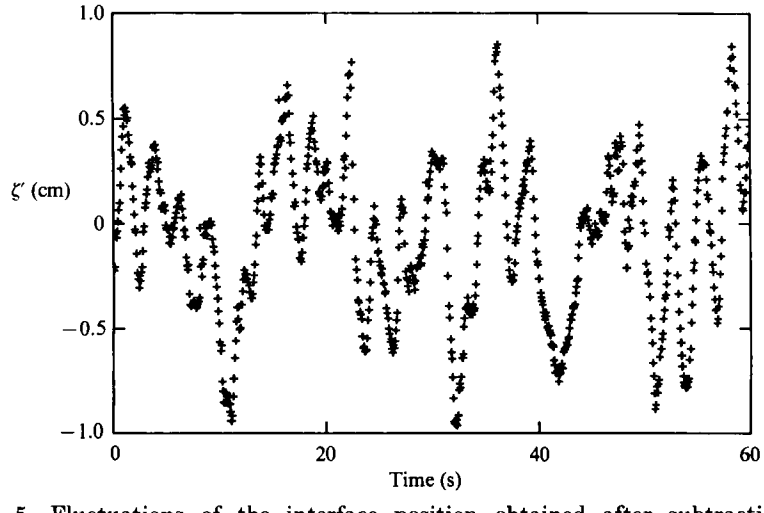

FIGURE 5. Fluctuations of the interface position obtained after subtraction of the mean displacement of the interface. ($\Delta\rho/\rho = 1.15\%$, $S = 3$ cm, $n = 6$ Hz, $\Omega = 0.3\pi$ rad s^{-1}.) The distance of the interface from the grid midplane is $D = 14.3$ cm.

4. Qualitative observations

The visualizations were made with the distance $D(t)$ of the interface from the grid midplane greater than Z_R. The interface is in that part of the tank where the effect of rotation is most significant: the structure of turbulence is quasi-two-dimensional,

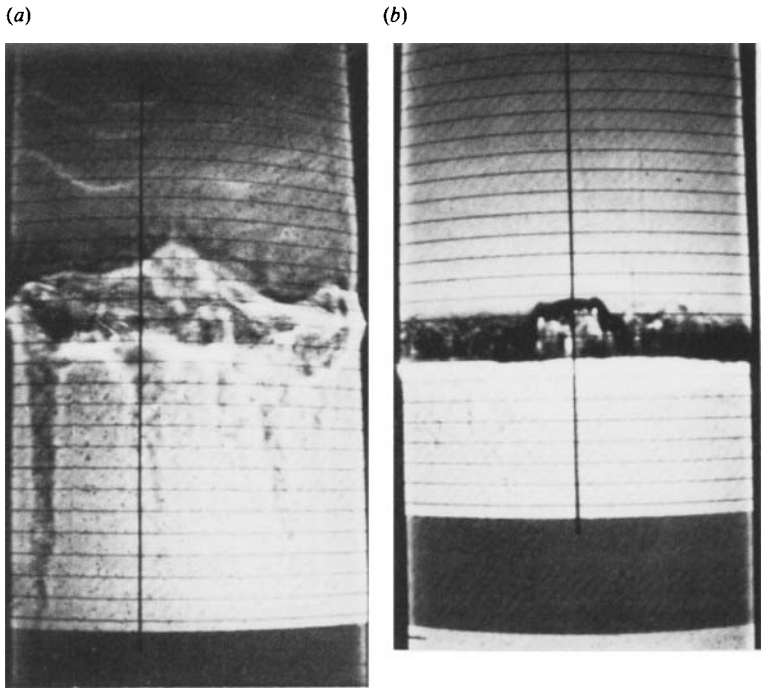

FIGURE 6. Shadowgraphs of the density field. Grid oscillation conditions are: $S = 4$ cm, $n = 6.6$ Hz. The distance between horizontal lines is 1 cm. (*a*) With rotation $\Omega = \pi$ rad s^{-1}, $\Delta\rho/\rho = 3.9\%$, $Ri = 29.5$. (*b*) Without rotation, $\Delta\rho/\rho = 3.0\%$, $Ri = 22.7$.

and intense and very concentrated vortices are generated (Hopfinger *et al.* 1982). Figure 6 compares shadowgraph pictures of the density field in rotating (figure 6*a*) and non-rotating (figure 6*b*) conditions. Richardson numbers were about $Ri \approx 25$ in the two cases. Deformations of the interface are more pronounced for rotating than for non-rotating conditions. This is due to pressure variations that are larger for rotating conditions ($p \approx \rho 2\Omega l u$ according to the geostrophic scaling) than for non-rotating conditions ($p \approx \rho u^2$). The balance of potential energy variation $\Delta\rho g A$ (A is the typical vertical displacement of the interface) with the pressure variations gives a typical vertical displacement of the order of $A/l \approx Ri^{-1}$ and $A/l \approx Ro^{-1}Ri^{-1}$ for non-rotating and rotating turbulence, respectively. The latter quantity is larger than the first when the Rossby number is small. In rotating conditions this scaling is valid outside the intense and concentrated vortices but the deformation of the interface caused by them is even more pronounced. Figure 6(*a*) shows long columns of light fluid which penetrate deeply into the cores of the intense vortices present in the mixing layer. The radius ϵ of the vortex cores is about 1.5 mm, while the rotation ω_c of the vortex is about 40 times the ambient rigid-body rotation (Hopfinger *et al.* 1982). Assuming that the fresh water contained at the centre of the cores is in hydrostatic equilibrium, a Rankine vortex model predicts that the length d of these columns is $d \approx \omega_c^2 \epsilon^2 / g' \approx 10$ cm for the conditions of figure 6(*a*). This estimate is consistent with observations.

In an experiment similar to ours, Noh & Long (1987) observed significant modifications of the interface under the effect of rotation when

$$\Omega(D_0/g')^{\frac{1}{2}} > 1.4 \tag{16}$$

(D_0 is the initial position of the interface). Important vortical motions appeared

(*a*)

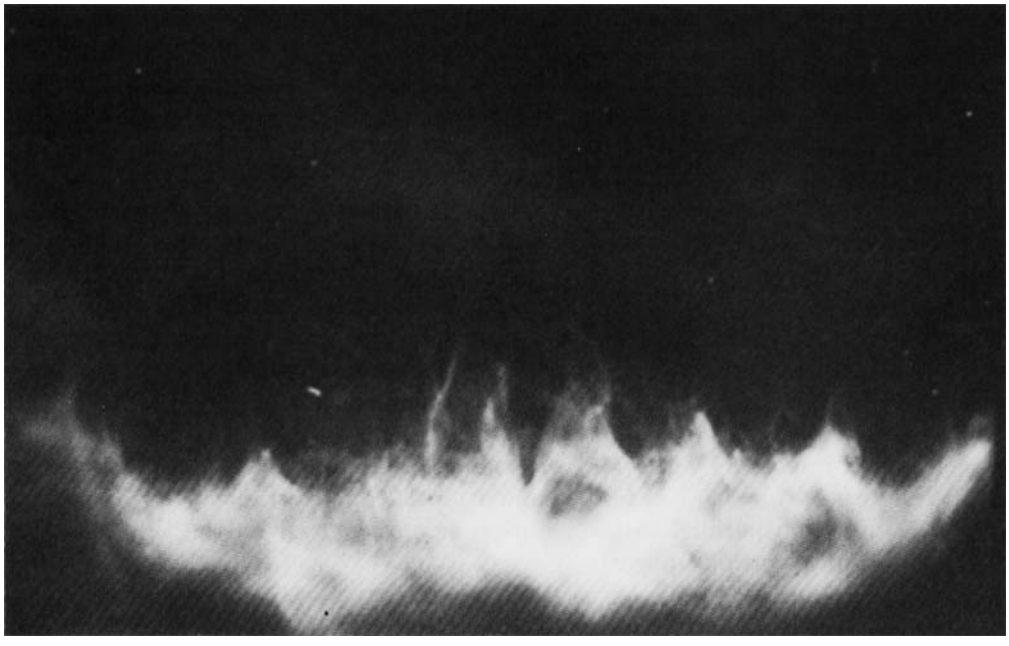

(*b*)

FIGURE 7. Variation of the density interface marked by fluoresceine dye by a vertical sheet of light parallel to the rotation axis. Experimental conditions are: $\Omega = \pi$ rad s^{-1}, $S = 4$ cm, $n = 6.6$ Hz. The distance of the interface from the grid midplane is $D = 30$ cm. (*a*) $\Delta\rho/\rho = 0.5\%$, $Ri = 4.5$; (*b*) $\Delta\rho/\rho = 1.5\%$, $Ri = 13.5$.

inside the non-mixed layer and the interface showed 'spike-like' patterns. Such observations were not made in our experiments, at least for the value predicted by Noh & Long. Figures 7 (*a*) and 7 (*b*) show photographs of the fluid in a vertical sheet of light, taken during an experiment for which the salty water was initially coloured by fluoresceine dye ($D_0 = 25$ cm). Values of the parameter $\Omega(D_0/g')^{\frac{1}{2}}$ are respectively 7.0 and 4.0 for these two pictures. The phenomenon described by Noh & Long seems to occur in figure 7 (*a*), but no 'spike-like' pattern is visible in figure 7 (*b*). To explain the quantitative discrepancy between Noh & Long's criterion and our observations, we suggest that their criterion is not sufficiently general for application to experiments different from theirs. We would expect that rotation modifies drastically the dynamics of the interface and the state of the non-mixed layer when the horizontal lengthscale of turbulence $l(D)$ at the interface is greater than the characteristic internal deformation radius. The lengthscale of turbulence should therefore enter in the criterion proposed by Noh & Long. We should also mention that the Richardson numbers is rather small in figure 7 (*a*) ($Ri = 4.5$) and larger in figure 7 (*b*) ($Ri = 13.5$). The constraint imposed by the stratification is therefore very weak for the flow shown in figure 7 (*a*). With rotation, momentum is rapidly transported by inertial waves in a direction parallel to the rotation axis, as shown by the thin sheets of coloured fluid propagating upward.

5. Entrainment rates

Entrainment rates were measured for three different conditions:

(i) for non-rotating conditions which served to establish a quantitative reference for entrainment rates in non-rotating conditions for comparison with experiments with rotation in the same apparatus and to verify the capability of our ultrasonic system. A comparison with previously published results (in particular E & Hopfinger 1986) was also made;

(ii) with rotation, with the distance of the interface from the grid midplane being less than Z_T. The Rossby numbers is rather high ($Ro > 0.2$). Turbulent velocity profiles are not noticeably modified by rotation (see §2.2), but the magnitude of the Coriolis force is sufficient to motivate a study of the effect of rotation on mixing for these conditions;

(iii) with rotation, with the distance of the interface from the grid midplane being greater than Z_R. The Rossby number is $Ro = 0.11$. Entrainment rates were determined in this case from shadowgraphs, because measurements by the ultrasonic technique failed. When the interface was located in this part of the tank, the ultrasonic signal delivered by the apparatus showed sudden jumps when intense vortices crossed the ultrasonic wave path (see §4 for a description of these vortices; the deformation of the interface caused by them is considerable). Only parts of the recordings could therefore be analysed. They were used to study interface oscillations (see §6) but the mean displacement of the interface could not be obtained.

5.1. *Entrainment in non-rotating flow*

Typical changes in the position of the interface without rotation are shown in figure 4 for the two grid oscillation conditions. In the log–log scales of the figure, the data can be closely fitted by a straight line, implying that a power function $D(t) = Ct^a$ (equation (14)) represents the mean displacement of the interface. It is straightforward to show from (15), (3) and (4) that the entrainment law is of the form

$$E(D) = u_e(D)/u(D) = K\,Ri(D)^{-p}, \tag{17}$$

$\Delta\rho/\rho$ beginning (%)	$\Delta\rho/\rho$ end (%)	a	C	C^*	p	K	K^*	Range of validity D (cm)	Range of validity Ri
				$S = 3$ cm, $n = 6$ Hz					
1.68	1.35	0.152	6.50	6.41	1.526	1.89	1.71	9.3–19.7	8.9–84.9
1.25	1.30	0.152	6.69	6.62	1.526	1.84	1.71	9.4–20.8	8.1–87.7
1.04	0.90	0.151	6.98	6.87	1.541	1.61	1.44	11.3–20.5	107.–63.6
0.93	0.85	0.148	7.18	6.95	1.586	1.72	1.35	9.5–20.6	5.8–59.2
				$S = 4$ cm, $n = 6.6$ Hz					
1.35	1.33	0.176	9.23	10.3	1.227	0.75	1.64	15.0–25.0	3.8–17.4
1.68	1.48	0.178	8.92	10.1	1.206	0.72	1.74	14.3–25.3	3.7–20.5
1.28	1.30	0.183	8.77	10.2	1.115	0.53	1.45	14.5–25.8	3.3–18.4

TABLE 1. Experimental conditions and results on entrainment rates in non-rotating fluid. The mean position of the interface varies according to $D(t) = Ct^a$ and the entrainment law is in the form $E = KRi^{-p}$. The coefficients C^* and K^* indicate data obtained when p is set to $\frac{3}{2}$ (thus $a = 0.154$). The density measured at the end of each experiment is in general slightly lower than before the grid oscillation is started. This is indicative of a small salt flux inside the non-mixed layers which is believed to occur mainly at the beginning of grid oscillation. The second value is therefore used to estimate the Richardson numbers.

because the entrainment rate is a function only of the Richardson number estimated at the position of the interface. Coefficients entering in the entrainment law are

$$p = (1-2a)/3a, \tag{18}$$

$$K = \frac{aC^{1/a}}{n}(S^3M)^{-1/4a}K_1^{(a-2)/3a}K_2^p\left(\frac{g'}{n^2S^3_4M^1_4}\right)^p. \tag{19}$$

Entrainment rates were measured for the two grid oscillation conditions ($S = 4$ cm, $n = 6.6$ Hz) and ($S = 3$ cm, $n = 6$ Hz). Data were analysed using $K_2 = 0.14$ for the former and $K_2 = 0.25$ for the latter. In both cases $K_1 = 0.26$. Values obtained for a, C, p and K in several experiments are summarized in table 1. The magnitude of entrainment obtained in different experiments is compared by estimating the value of K, when the exponent p is fixed at $\frac{3}{2}$ (thus $a = 0.154$). The corresponding values of C and K, denoted C^* and K^*, are also reported in table 1. The choice of the two different values of K_2 for the two different grid oscillation conditions gives consistent entrainment rates for these two conditions. E & Hopfinger (1986) also varied the value of K_2 in the range 0.1–0.25 to collapse on a single curve entrainment rates obtained for different values of the grid characteristics S/M. Since the general variation of K_2 with S/M is not known, the use of different values of K_2 is quite empirical, though Mory & Hopfinger (1985) measured $K_2 = 0.14$ for ($S = 4$ cm, $n = 6.6$ Hz) and Hopfinger & Toly (1976) obtained $K_2 = 0.25$ for various grid characteristics.

For the conditions of grid oscillation given by ($S = 3$ cm, $n = 6$ Hz), the exponent $p = \frac{3}{2}$ predicted by Linden (1973) is confirmed. For the grid oscillation conditions ($S = 4$ cm, $n = 6.6$ Hz), the exponent p of the entrainment law is about 1.2, which is smaller than $\frac{3}{2}$. This departure, which was observed in several experiments (see table 1), is certainly representative of some change in the mixing process or in the turbulence structure. Other authors (Nokes 1988, among others) have reported a similar exponent in the entrainment law. We also notice that the Richardson number

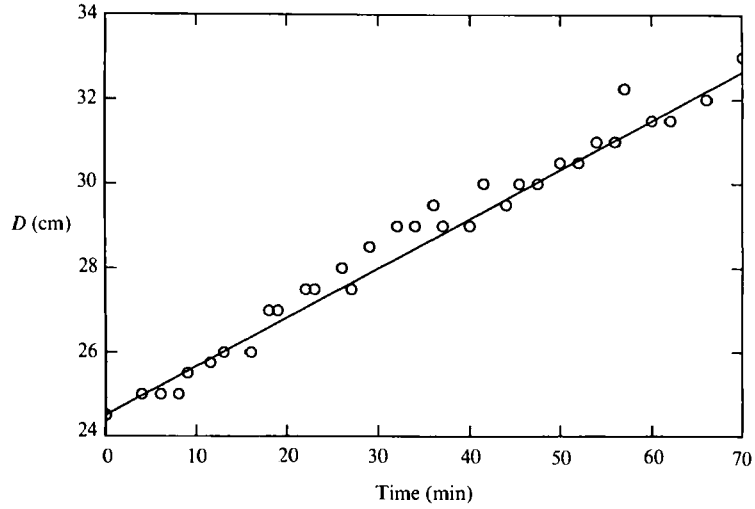

FIGURE 8. Mean displacement of the interface in the domain of the tank $D > Z_R$, where turbulence is quasi-two-dimensional. Experimental conditions are: $\Omega = \pi$ rad s^{-1}, $S = 4$ cm, $n = 6.6$ Hz, $\Delta\rho/\rho = 5.3\%$, $Ri = 44.5$.

is quite low during the experiments with the conditions ($S = 4$ cm, $n = 6.6$ Hz), implying that Linden's model (which relies on $Ri \gg 1$) may not be representative.

Most of our data on entrainment measured in rotating conditions have been obtained with the grid oscillation conditions ($S = 3$ cm, $n = 6$ Hz). The grid characteristics ($S = 4$ cm, $n = 6.6$ Hz) are only used when the interface is located in the domain $D(t) > Z_R$ (§5.3), but the Richardson numbers are in this case much higher than those achieved for the corresponding experiments without rotation. We therefore approximate the entrainment law in non-rotating conditions in the following by $E = 1.6Ri^{-\frac{3}{2}}$.

5.2. *Entrainment in rotating flow for Ro < 0.2*

The interface is located in the domain of the tank where turbulence is quasi-two-dimensional. The Rossby number is constant. The Richardson number is also almost constant. Its variation during an experiment, caused by the change in g' as the interface moves (configuration A was used for this series of experiments), is less than 15% for the smallest Richardson number considered ($Ri = 7.6$) and less than 3% for the highest ($Ri = 44.5$). The dependency of entrainment rates on the Richardson number was obtained by changing the initial density difference between the two layers for each experiment.

Figure 8 shows a typical shift in the mean position of the interface, as determined from an experiment by the observation of a shadowgraph movie. Clearly, the advance of the interface $D(t)$ is well described by a linear time function, implying that the entrainment velocity is approximately constant during an experiment, when the interface is located in the quasi-two-dimensional domain of the tank ($D(t) > Z_R$). This result is to be expected, because the Rossby number and the Richardson number are almost constant during an experiment. We can therefore satisfactorily estimate the entrainment velocity u_e from the slope of the straight line fitting the data (as shown in figure 8), and the characteristic Richardson number is determined from the mean density jump during the period of time considered. The velocity $u(Z_R)$ and lengthscale $l(Z_R)$ were taken from (5) and (6), respectively. The conditions and

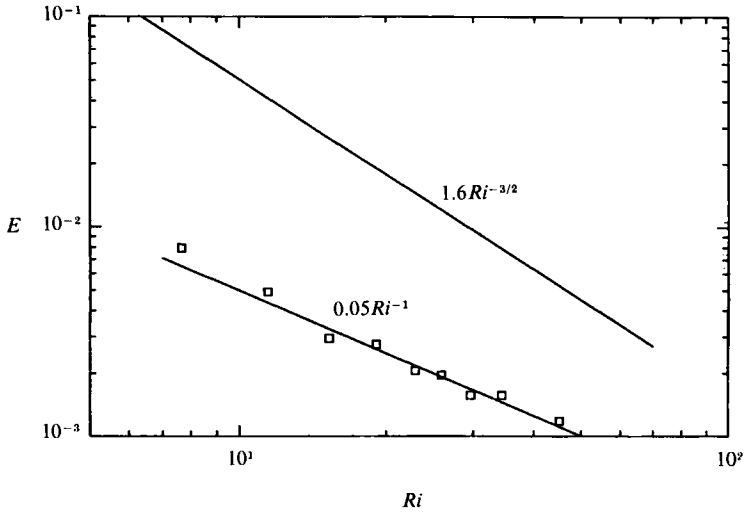

FIGURE 9. Entrainment rates versus the Richardson number, when the interface is in the domain $D > Z_R$ (quasi-two-dimensional domain), compared to entrainment rates obtained in non-rotating conditions ($E = 1.6Ri^{-\frac{3}{2}}$). Experimental conditions are: $\Omega = \pi$ rad s^{-1}, $S = 4$ cm, $n = 6.6$ Hz ($Ro = 0.11$).

$\Delta\rho/\rho$ (%)	$\Delta\rho/\rho$ (%)	Ri	u_e (cm/mn)	$E = u_e/u$
1.00	0.90	7.6	0.81	7.94×10^{-3}
1.50	1.35	11.4	0.50	4.90×10^{-3}
2.00	1.80	15.1	0.30	2.94×10^{-3}
2.50	2.25	19.0	0.28	2.75×10^{-3}
3.00	2.70	22.7	0.21	2.06×10^{-3}
3.40	3.05	25.3	0.20	1.96×10^{-3}
3.90	3.50	29.5	0.16	1.57×10^{-3}
4.50	4.05	34.0	0.16	1.57×10^{-3}
5.80	5.30	44.5	0.12	1.18×10^{-3}

TABLE 2. Experimental conditions on entrainment rates for rotating conditions obtained when the interface is in the domain $D(t) > Z_R$. The first value of the density jump was measured at the beginning of the experiment. The second value is the mean density jump during an experiment, and was used to estimate the Richardson number. The Rossby number is $Ro = 0.11$.

results obtained for nine experiments with different density jumps are summarized in table 2. The Rossby number is $Ro = 0.11$ for all experiments. The entrainment rates E obtained for this series of experiments are represented in figure 9 as a function of the Richardson number. It was noted in §4 that the appearance of the mixing mechanism completely changes for Richardson numbers below about 4.5–7.5, where mixing becomes more rapid. When only the entrainment rates for Richardson numbers in the 10–45 range are considered, the data closely fit the law

$$E = 0.05Ri^{-1}. \tag{20}$$

The comparison, in figure 9, of this mixing law with the mixing law in non-rotating turbulent flow ($E = 1.6Ri^{-\frac{3}{2}}$), shows that rotation decreases the mixing rate for a given Richardson number.

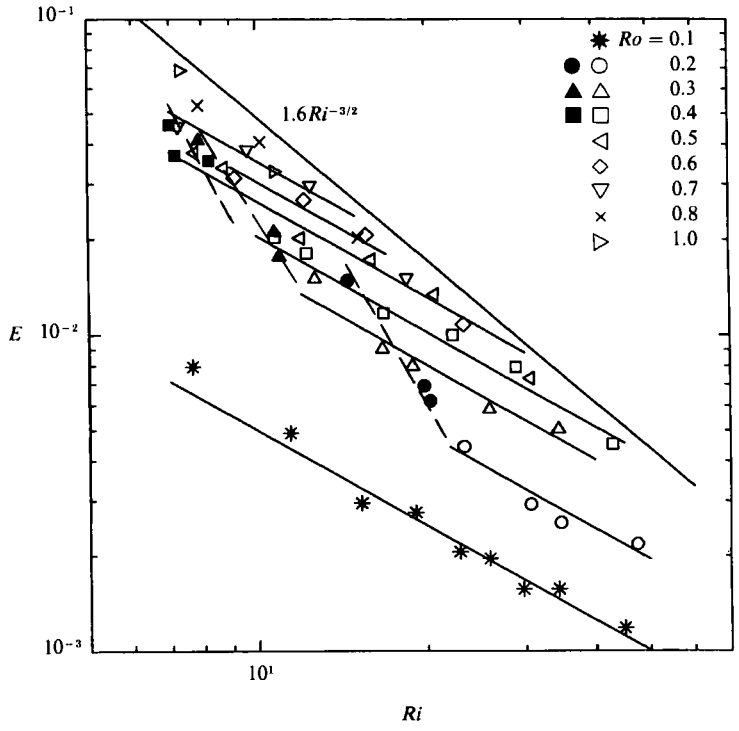

FIGURE 10. Entrainment rates when the interface is in the domain $D < Z_T$ ($Ro > 0.2$). The dependence on Richardson and Rossby numbers is given. Open symbols indicate data showing an Ri^{-1} dependence of the entrainment rate (solid lines). Those data showing a departure from this relation are filled and joined together by dotted lines. Experimental conditions are $S = 3$ cm, $n = 6$ Hz. The upper solid line marks the entrainment law obtained in non-rotating conditions. The * indicate results for $Ro = 0.11$ ($D > Z_R$).

5.3. *Entrainment in rotating flow for Ro > 0.2*

In these experiments the distance $D(t)$ of the interface from the grid midplane is less than Z_T. A typical ultrasonic recording of the displacement of the interface as a function of time is included in figure 4 (curve *c*). A power function $D(t) = Ct^a$ satisfactorily represents the data, as in the non-rotating case. The Richardson and Rossby numbers vary during an experiment as $D(t)$ increases:

$$Ri(D) = \frac{K_2}{K_1^2}\frac{g'}{Mn^2}\left(\frac{D}{S}\right)^3, \tag{21}$$

$$Ro(D) = \frac{K_1}{K_2}\frac{n}{2\Omega}\frac{S^{\frac{3}{2}}M^{\frac{1}{2}}}{D^2}, \tag{22}$$

with $K_1 = 0.26$ and $K_2 = 0.25$ (grid oscillation conditions are $S = 3$ cm and $n = 6$ Hz).

Following Maxworthy (1986), entrainment rates $E = u_e/u$ are plotted as a function of the Richardson number, keeping the Rossby number constant. They are estimated, after experimental determination of the constants C and a, from (15) and (3) taken at the positions of the interface corresponding to given values of the Rossby number. The Richardson number for this position of the interface was then deduced

$\Delta\rho/\rho$ (%) beginning	$\Delta\rho/\rho$ (%) end	Ω rad s^{-1}	Z_T (cm)	a	C	$D(t)$ (cm)	Ri	Ro
1.36	1.15	0.1π	24.0	0.158	6.253	9.4–18.3	7.3–53.6	1.3–0.34
1.24	1.15	0.13π	21.1	0.149	6.625	9.7–16.1	8.0–36.5	0.94–0.34
1.19	1.10	0.15π	19.6	0.147	6.605	9.9–17.5	8.1–44.9	0.78–0.25
1.30	1.28	0.2π	17.0	0.146	6.139	9.3–18.4	7.8–47.7	0.67–0.20
1.43	1.30	0.25π	15.2	0.131	6.497	9.6–16.6	8.8–34.7	0.50–0.20
1.18	1.15	0.25π	15.2	0.132	6.566	9.5–16.1	7.5–30.7	0.51–0.20
1.28	1.15	0.3π	13.9	0.125	6.801	9.7–16.1	8.0–23.5	0.41–0.20
0.99	1.00	0.3π	13.9	0.140	6.442	9.9–14.9	7.4–20.4	0.39–0.20
0.98	0.98	0.3π	13.9	0.134	6.795	10.3–16.3	8.1–19.9	0.36–0.20
1.10	1.10	0.4π	12.0	0.142	6.489	10.2–16.1	8.9–14.5	0.28–0.20

TABLE 3. Experimental conditions and results on entrainment rates in rotating fluid, obtained when the interface is in the domain $D(t) < Z_T$ ($S = 3$ cm, $n = 6$ Hz). The mean position of the interface varies according to $D(t) = Ct^a$. Density is given at the beginning and at the end of each experiment.

from (21) (configuration B was used for these experiments, implying that g' is constant during an experiment).

The results are represented in figure 10, showing the entrainment rate versus the Richardson number for nine values of the Rossby number, ranging from 0.2 to 1. Table 3 summarizes the experimental conditions from which figure 10 was established. For the non-rotating experiments, the density difference at the end of each run was used to calculate the Richardson number. The Richardson-number range covered is 7–50, but the range is narrower for experiments with the highest rotation rates. For the latter, the position of the transition Z_T is closer to the grid so that only part of the data $D(t)$, corresponding to $D(t) < Z_T$, can be interpreted. The entrainment law for non-rotating conditions $E = 1.6Ri^{-\frac{3}{2}}$ is included in this figure, as well as data obtained when $D(t) > Z_R$ (quasi-two-dimensional turbulence, see §5.2 and figure 9). Interesting conclusions may be drawn from figure 10. A decrease of the entrainment rate is always observed under the effect of rotation. A significant departure from the non-rotating entrainment law appears when $Ro < 0.6$, and the decrease is more pronounced when $Ro < 0.3$. With rotation, the variation of the entrainment rate with the Richardson number (for constant Rossby number) is less rapid than for the non-rotating condition. For Rossby numbers below 0.6, straight lines resulting from $E \propto Ri^{-1}$ satisfactorily fit the data in a certain range of Richardson numbers (unfortunately, this range of adjustment corresponds in general only to a variation of the Richardson number by a factor of 3). When the Richardson number is below a critical value, which depends on the Rossby number, a sudden increase of the entrainment rate is observed in figure 10 (data represented by filled symbols and joined together by dotted lines for each Rossby number). The determination of the dependency of this critical Richardson number on the Rossby number remains speculative in view of the small amount of data available. At the highest Richardson numbers, entrainment rates in rotating conditions never seem to exceed those of non-rotating conditions, as should happen if the $E \propto Ri^{-1}$ and $E \propto Ri^{-\frac{3}{2}}$ entrainment laws held respectively in rotating and non-rotating conditions for sufficiently high Richardson numbers. In particular, the experimental points for $Ro = 0.5$ and $Ro = 0.6$, shown in figure 10, no longer vary like Ri^{-1} for the highest Richardson numbers, but rather like $Ri^{-\frac{3}{2}}$, as in non-rotating mixing. In spite of the lack of data for large Richardson numbers, it seems likely that the upper bound for

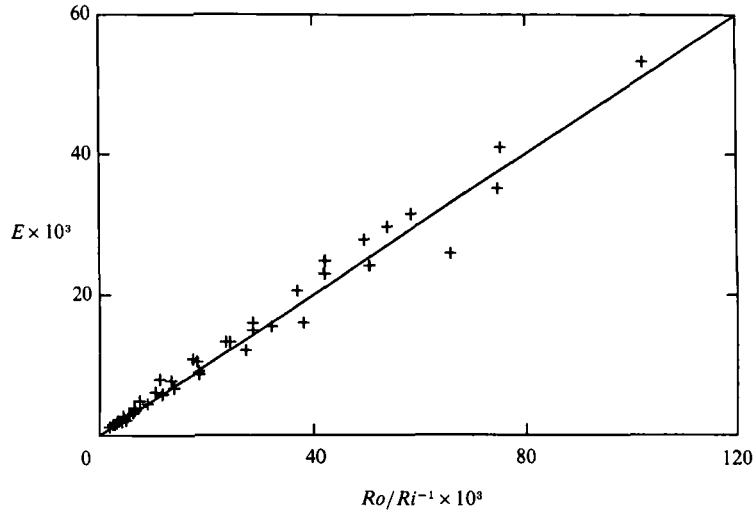

FIGURE 11. Entrainment rates when the interface is in the domain $D < Z_T$. This plot uses the data of figure 10.

the Richardson-number range in an entrainment law of the form $E = K(Ro)\,Ri^{-1}$ will be given by the point at which this relation intersects with the non-rotating relation $E = 1.6Ri^{-\frac{3}{2}}$.

To illustrate more clearly the fit of an entrainment law of the form $E = K(Ro)\,Ri^{-1}$ with the data, and subsequently determine the function $K(Ro)$, the data in figure 10, showing such a dependence, are replotted in figure 11 as a function of the parameter $Ro\,Ri^{-1}$. A linear function provides a good approximation of the results. The entrainment rates can therefore be estimated as a function of the single parameter $Ro\,Ri^{-1} = u^3/g'l^2f$ in the range considered, which is very wide (a factor of 30). The entrainment law in rotating conditions can therefore be represented in the form

$$E = 0.5Ro\,Ri^{-1}. \tag{23}$$

This is a correct approximation for all conditions considered in this study, including conditions for $D(t) > Z_R$ as well as for $D(t) < Z_T$.

6. Interface displacement spectra

Mean frequency spectra of the fluctuating displacements of the interface were obtained using the ultrasonic system in the three typical conditions for which entrainment rates were determined in §5. If $\zeta(t)$ designates the instantaneous displacement of the interface (after subtraction of the mean displacement) and $\hat{\zeta}(\omega)$ is Fourier transform in the frequency domain, the averaged interface displacement frequency spectrum $\Phi(\omega)$, called 'internal wave spectrum' by Hannoun & List (1988), is expressed as

$$\Phi(\omega) = \langle \hat{\zeta}(\omega)\,\hat{\zeta}^*(\omega) \rangle, \tag{24}$$

$\langle\,\rangle$ being the ensemble average. The dimensions of the interface displacement spectrum will be given in units of cm^2 s. Integration of this spectrum with respect to frequency leads to the mean-square amplitude of fluctuations of the interface position. The method for obtaining the spectra was described in detail in §3. In the present section we present the spectra, provide estimates of the typical frequencies characterizing the flow (turbulent frequency, internal wave frequency, Brunt–

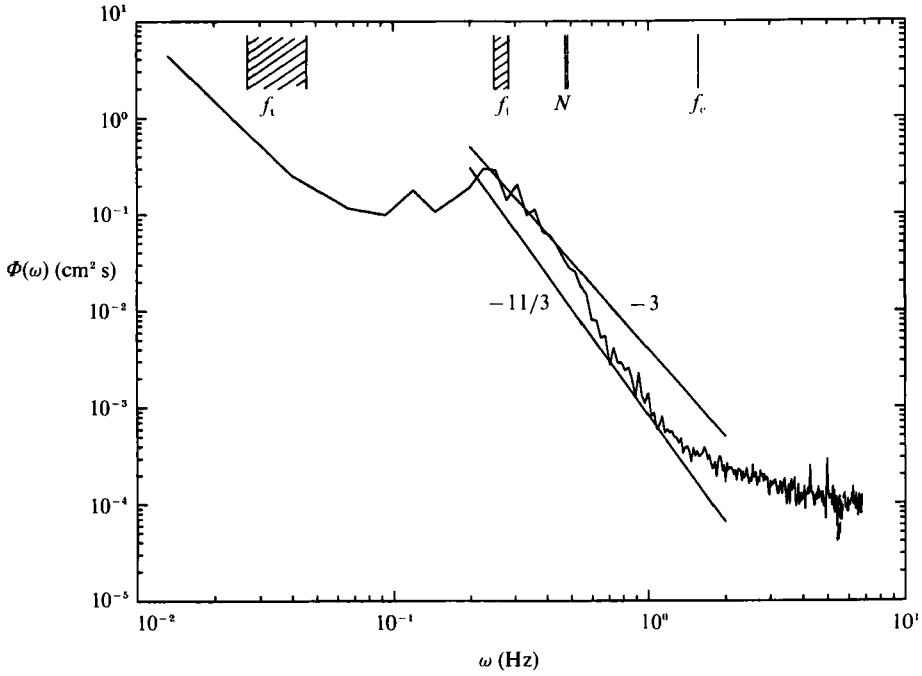

FIGURE 12. Interface displacement spectrum measured in non-rotating conditions. Experimental conditions are $S = 3$ cm, $n = 6$ Hz, $\Delta\rho/\rho = 1.3\%$. The spectrum is averaged over a time period during which the mean position of the interface moves from $D = 15.8$ cm ($Ri = 39$) to $D = 20.5$ cm ($Ri = 84$).

Väisälä frequency), and prepare for the discussion of §8. The frequency spectra are Eulerian spectra and characterize interface oscillations at a fixed position in the tank. Frequencies ω are related to the wavenumber k characterizing the spatial scales of turbulent eddies by $\omega = uk$, u being the horizontal r.m.s. turbulent velocity.

The interface displacement spectra are presented in figures 12–14. Two of them were measured in rotating conditions, when the distances of the interface from the grid are respectively greater than Z_R (figure 14) or about Z_T (figure 13). For the latter case the interface position is actually $Z_T \leqslant D(t) \ll Z_R$. Entrainment rates were not determined in this part of the tank, but the interface oscillation can be studied without recourse to any assumption concerning the structure of turbulence since the mean displacements of the interface are known. We believe that the spectrum obtained does not differ to any great extent from that measured when $D(t)$ is just smaller than Z_T. On the other hand the spectrum in figure 12, measured without rotation, will serve as a reference state for the rotating experiments. Interface displacement spectra were measured only recently in an experiment similar to ours by Hannoun & List (1988); a comparison with their results seems useful.

On each diagram, frequencies determined from the experimental conditions are marked to define characteristic frequency ranges. The rotation frequency (in figures 13 and 14) is Ω/π. Other typical frequencies are the turnover frequency of turbulence, the frequency of internal waves and the Brunt–Väisälä frequency. For an internal wave at a density interface of thickness equal to zero, the angular frequency $\omega = 2\pi f_i$ (f_i is the internal wave frequency) is related to the wavenumber $k = 2\pi/\lambda$ (λ is the wavelength) by

$$\omega = 2\pi f_i = (g'k)^{\frac{1}{2}} = (g'2\pi/\lambda)^{\frac{1}{2}}. \tag{25}$$

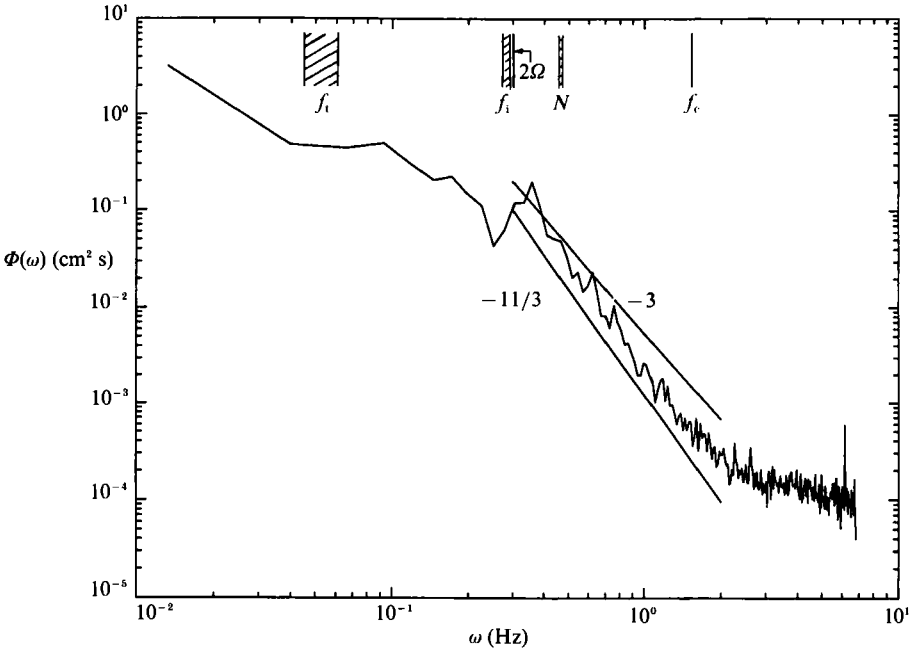

FIGURE 13. Interface displacement spectrum measured in rotating conditions ($D \approx Z_T$). Experimental conditions are $\Omega = 0.3\pi$ rad s^{-1}, $S = 3$ cm, $n = 6$ Hz, $\Delta\rho/\rho = 1.15\%$. The spectrum is averaged over a time period during which the mean position of the interface moves from $D = 13.8$ cm ($Ri = 23$, $Ro = 0.24$) to $D = 16.1$ cm ($Ri = 36.5$, $Ro = 0.18$).

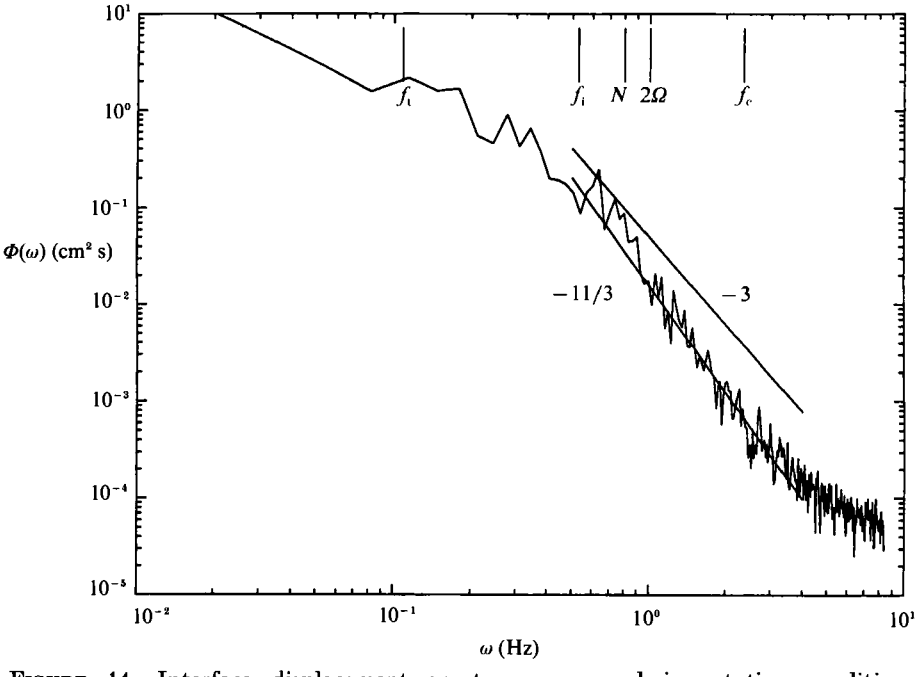

FIGURE 14. Interface displacement spectrum measured in rotating conditions ($D > Z_R$). Experimental conditions are $\Omega = \pi$ rad s^{-1}, $S = 4$ cm, $n = 6.6$ Hz, $\Delta\rho/\rho = 2.8\%$, $Ri = 23.6$, $Ro = 0.11$.

A typical wave field has spatial and temporal variations in the form

$$u(t,x,z) = U(z)\cos(kx-\omega t) \tag{26}$$

(u is the horizontal velocity component, parallel to x). The correlation lengthscale of this velocity field, when it is defined in the same way as for a turbulent velocity field, is

$$l = \frac{1}{U^2(z)\cos^2(\omega t)}\int_0^{\lambda/4} u(t,0,z)\,u(t,x,z)\,\mathrm{d}x = \frac{\lambda}{2\pi}. \tag{27}$$

The most energetic turbulent motions take place at the typical correlation lengthscale determined by the integral lengthscale. We expect that the most energetic internal waves will also be generated at this lengthscale. Equations (25) and (27), therefore, define the characteristic frequency of internal waves as

$$f_\mathrm{i} = (1/2\pi)(g'/l)^{\frac{1}{2}}. \tag{28}$$

The Brunt–Väisälä frequency $N = (1/2\pi)(g'/e)^{\frac{1}{2}}$ is the cutoff frequency for the propagation of internal waves. It is estimated using the averaged interface thickness e. The interface thickness could not be obtained by our ultrasonic device. Measurements by E & Hopfinger (1986), performed in the absence of rotation, are therefore used: $0.28 < e/l < 0.4$ for Richardson numbers in the range $20 < Ri < 50$ (figure 7 of their paper, interpreted with $l = 0.25D$), while the asymptotic value for very large Richardson numbers is $e/l \approx 0.22$. The ratio of the Brunt–Väisälä frequency to the internal wave frequency f_i is therefore of order $N/f_\mathrm{i} \approx 1.5$–$2.2$. In non-rotating conditions, internal waves are produced at frequencies smaller than the Brunt–Väisälä frequency N. The most energetic oscillations are generated by turbulent eddies with lengthscale of the order of $2\pi l$ producing oscillations at the frequency f_i. It is therefore expected that interface displacement spectra will show a peak at the frequency f_i.

The turbulent eddy turnover frequency f_t, characterizing the turbulent timescale, is $f_\mathrm{t} = u/(2\pi l)$. The $1/2\pi$ proportionality constant is introduced because it is more appropriate to define the turbulent inertial frequency from a physical lengthscale of motion λ than from a correlation lengthscale l. The order of magnitude of the ratio between the two is 2π, as determined from (27). Moreover, introducing the $1/2\pi$ constant to define the turbulent frequency makes sense physically when the characteristic frequencies of internal waves and turbulence are compared; we in fact verify that $f_\mathrm{i}/f_\mathrm{t} = Ri^{\frac{1}{2}}$.

In figures 12–14, some frequencies are indicated by narrow bands. The frequency spectra have been averaged by considering the oscillations of the interface over a long period of time (several minutes, see §3). During this period, the mean position of the interface changes and the values of the characteristic frequencies vary (except for figure 14, which concerns oscillations when the interface is located in the quasi-two-dimensional part of the tank). There is significant variation in the turbulent frequency, but little in the internal wave and Brunt–Väisälä frequencies. The dynamics of interface displacement fluctuations do not vary much during the period of time considered in the frequency range limited by the last two frequencies.

The last frequency indicated in figures 12–14 is the cutoff frequency of the measured oscillations, imposed by the size of the piezoelectric oscillator (8 mm × 8 mm). The smallest wavelength λ_c of an internal wave that can be analysed is thus $\lambda_\mathrm{c} = 0.8$ cm. The cutoff frequency, estimated from (25), is $f_\mathrm{c} = (g'/2\pi\lambda_\mathrm{c})^{\frac{1}{2}}$. This is significantly higher than all frequencies given above for all cases considered. We

verify in figures 12–14 that f_c is the frequency above which the data show random noise. In spite of the rather large size of the piezoelectric oscillator used as ultrasonic wave emitter, the frequency analysis, also confirmed by the experimental data, ensures that our system is able to capture the dynamics of the interface in the required range.

The frequency interface displacement spectrum in non-rotating conditions (figure 12) is in agreement with the previous observations by Hannoun & List (1988, figures 12 and 13). The most significant oscillations of the interface are at frequencies representative of internal waves, whereas oscillations at frequencies characteristic of turbulence remain small. We conclude, as other authors have done, that the response of the interface to perturbations caused by turbulence is driven by an internal wave dynamic. For frequencies above f_i (the amplitude of oscillations is maximum for $\omega \approx f_i$) the oscillations decrease. A straight line with a slope of $-\frac{11}{3}$ is indicated in figures 12–14, with reference to a model proposed by Mory (1991). A straight line with slope -3 is also shown on the diagram. This refers to the theory of Phillips (1977) predicting a $\Phi(\omega) \propto \omega^{-3}$ decrease in the internal wave spectrum in the frequency range $f_i < \omega \ll N$. A deficiency of our experiment is the smallness of the ratio N/f_i; the range $f_i < \omega < N$ is too narrow to establish any particular form of the interface displacement spectrum. This deficiency is difficult to avoid because the interface tends naturally to thicken, when the experiment lasts for long time, and to reach a value of about $\frac{1}{3}$ of the integral lengthscale. Hannoun & List apparently encountered similar difficulties. For $R_j = 24$, the internal wave spectrum presented in their figure 12 is interpreted as a $\Phi(\omega) \propto \omega^{-3}$ spectrum extending over a decade and half, but figure 10 of their paper gives $N/f_i \approx 2.5$ and $e/l \approx 0.16$ for this condition. Their figure 10 also shows that the ratio N/f_i reaches higher values for the highest Richardson numbers studied ($N/f_i \approx 5$ for $R_j \approx 100$). This is not a large value, though Hannoun & List suggest that their apparatus underestimates N for $R_j > 50$ (p. 225).

The frequency interface displacement spectra obtained in rotating conditions (figures 13 and 14) display important modifications, in comparison with the non-rotating spectrum. The most significant novelty is that significant fluctuations of the interface occur at frequencies below f_i. The most energetic fluctuations of the interface occur at frequencies of the order of magnitude of the turbulent frequency (and smaller than the rotation frequency). For frequencies above f_i and Ω/π the spectra look similar in rotating and non-rotating conditions. In particular their slope is not modified.

An additional insight into the dynamics of the interface is obtained from the recordings of interface displacements by computing of the r.m.s. amplitude of oscillations A, and the r.m.s. vertical velocity component of the interface w_i. These quantities were determined during this study (Fleury 1988). Their variation is in accordance with $A/l \propto Ri^{-1}$ and $w_i/u \propto Ri^{-\frac{1}{2}}$, in agreement with the measurements by Hannoun & List.

7. Motion in the non-stirred layer

As noted in earlier studies (Noh & Long 1987; Maxworthy 1986) one major difference occurring when background rotation is applied to the flow, as compared with non-rotating flow, is the possibility of energy radiation into the non-stirred layer by inertial waves. These give rise to noticeable motions in this layer, which is almost quiescent in the absence of rotation when the Richardson number is high.

By analysing particle displacement streaks on photographs, in the manner

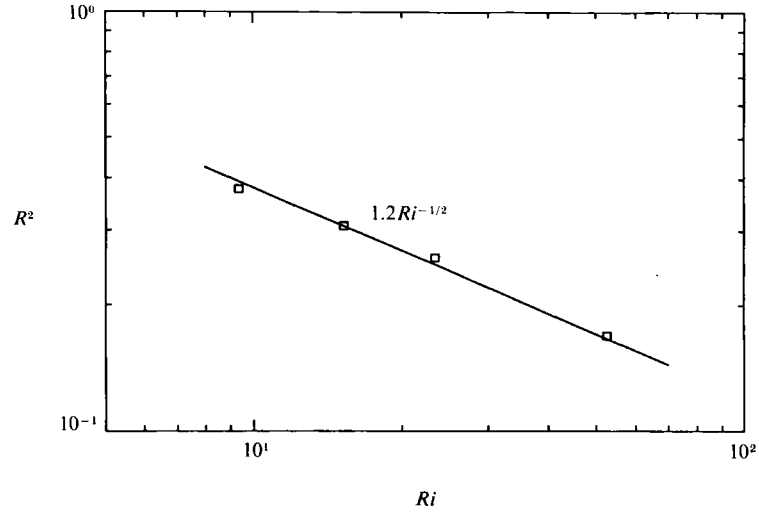

FIGURE 15. Ratio of the r.m.s. kinetic energies in the non-turbulent layer and the turbulent mixed layer. Experimental conditions are: $\Omega = \pi$ rad s^{-1}, $S = 4$ cm, $n = 6.6$ Hz, $D = 25$ cm.

described in §2.3, we determined the ratio $R^2 = u_{\mathrm{NM}}^2/u_{\mathrm{M}}^2$, comparing the r.m.s. kinetic energies per unit mass of the horizontal components of velocity in the non-mixed and mixed layers, denoted u_{NM}^2 and u_{M}^2 respectively. Experimental conditions are ($S =$ 4 cm, $n = 6.6$ Hz) and rotation rate $\Omega = \pi$ rad s^{-1}. The r.m.s. horizontal velocity in the non-mixed layer is measured by particle streaks illuminated by a sheet of light placed 40 cm from the grid and parallel to it. The distance of the interface from the grid is about 25 cm. The interface is therefore located in the part of the tank where the flow is quasi-two-dimensional, and motion in the non-mixed layer is also quasi-two-dimensional. The Rossby number characterizing the flow at the interface is at the minimum value achievable in our apparatus ($Ro = 0.11$), implying that energy transmission across the interface by inertial waves should be maximum. It was demonstrated in §5 that entrainment is significantly reduced in the presence of rotation, and proportional to Ro. The aim is now principally to determine whether energy radiation into the non-stirred layer is significant. We do not study the dependence of $R^2 = u_{\mathrm{NM}}^2/u_{\mathrm{M}}^2$ on Rossby number, but instead focus on experimental conditions where energy radiation is maximum. The r.m.s. horizontal kinetic energy per unit mass in the mixed layer u_{M}^2 is measured in one experiment without stratification. In the analysis of particle streaks the whole tank section is considered in order to prevent artificial over-estimation of velocity. The domain is divided into small squares by a regular mesh grid and an equal number of particles is taken in each square. When no particle is present in the square, the velocity is assumed to be zero. Indeed, particles with low velocity are generally less visible. By comparing the results with measurements by Hopfinger *et al.* (1983), we verify that this procedure correctly reproduces the velocity with good accuracy. In figure 15, the ratio R^2 is plotted versus the Richardson number Ri for $9 < Ri < 55$. The kinetic energy in the non-stirred layer is a significant fraction of the kinetic energy in the mixed layer (40% at $Ri = 9$ and 20% at $Ri = 50$).

8. Discussion

An experimental study was conducted to examine turbulent mixing across a density interface, when the fluid is subjected to rotation. Entrainment rates were determined. Insight into the mixing process was provided by the interface displacement spectra and by measurements of energy transmission across the interface.

Confirming the previous results obtained by Maxworthy (1986) and by Noh & Long (1987), we observed that rotation decreases the entrainment rate for a given Richardson number. The specific dependence of entrainment rates on the Rossby and Richardson numbers were not given by the latter authors. From our measurements we were able to correlate the data by the following entrainment law:

$$E = 0.5 Ro\, Ri^{-1}. \tag{29}$$

The decrease in entrainment rate as the Richardson number increases is therefore slower in rotating conditions than in the absence of rotation. In the latter case we give confirmation of

$$E = 1.6 Ri^{-\frac{3}{2}}. \tag{30}$$

In rotating conditions the entrainment law (29) is valid as long as the entrainment rate is less than predicted by the non-rotating entrainment law (30). This fixes an upper bound for the validity of entrainment relation (29) ($Ri < (3.2)^2 Ro^{-2}$). Owing to the very small amount of data available at high Richardson numbers, we could not verify whether the non-rotating entrainment law (30) is also representative of entrainment in rotating conditions, when the Richardson number is greater than $(3.2)^2 Ro^{-2}$. This is likely to happen, but cannot be demonstrated.

The decrease in entrainment rate and the change in form of the entrainment law under the effect of rotation show that the dynamics of mixing is strongly modified by rotation. The interface displacement spectra, presented in §6, confirm this result and display important new features of the effect of rotation on the dynamics of the interface. An important result is that the interface displacement spectra are not modified by rotation in the high-frequency range ($\omega > 2\Omega$). This property is used in the context of a new theory proposed by one of the authors (Mory 1991). This theory associates mixing with the small-scale eddies having sufficiently low Richardson numbers to mix the density profile. The mechanism of mixing is of Kelvin–Helmholtz-instability type. The entrainment laws $Ro\, Ri^{-1}$ and $Ri^{-\frac{3}{2}}$ obtained in the present study are recovered. In this model entrainment depends on the shape of the small-scale turbulent kinetic energy spectrum, which is related to the interface displacement spectrum. The slope of the interface displacement spectrum in the high-frequency range is examined in more detail by Mory (1991). This model predicts an interface displacement spectrum in the form $\Phi(\omega) \propto \omega^{-\frac{11}{3}}$ whereas Phillips (1977) obtains $\Phi(\omega) \propto \omega^{-3}$. Both theories are compared by Mory (1991).

Another important effect of rotation on interface oscillations shown by the interface displacement spectra is the increase of low-frequency oscillations ($\omega < 2\Omega$) at frequencies of the order of magnitude of the frequency of turbulence u/l. We relate the generation of these oscillations to the existence of inertial and internal waves. An initial explanation for the decrease in entrainment rate, suggested by Maxworthy (1986), was that radiation of kinetic energy by inertial waves across the interface reduces the amount of energy available for mixing. Our measurements of velocities in the non-stirred layer show that energy transmission across the interface is

significant when the fluid is subjected to rotation. This confirms the prominent part played by inertial waves in this flow. This may explain a decrease in the constant in (30), but is not consistent with a modification of the power law of the Richardson number. The role of inertial waves is essential for establishing flow when stirring of the mixed layer starts. However, when turbulence is established and statistically steady, inertial waves propagating upward across the interface are reflected by the upper boundary (the fluid layers in the experiments are of finite depth). A significant part of the energy transmitted into the non-stirred layer can therefore be fed back into the mixed layer. In non-rotating flows, internal waves are generated by the distortion of the interface by turbulent eddies of the size of the integral lengthscale l or smaller. The interface response timescale is of the order of $(\frac{1}{2}\pi)(g'/l)^{\frac{1}{2}}$ or more. Rotation permits the combination of internal and inertial waves, which can produce oscillations of the interface with the integral lengthscale l and the turbulent turnover time $2\pi l/u$ as typical timescale. These oscillations are in fact produced by turbulence as shown by the interface displacement spectra. Their amplitude proves the significant energy exchanges between the two layers, which are caused by inertial waves. However, according to Mory's (1991) theory, these low-frequency and large-scale oscillations should not take part in the mixing.

S. Layat, J. P. Barbier-Neyret and G. Brault are gratefully acknowledged for their technical assistance in the experimental part of this work. This program was supported by the Programme Atmosphère Météorologique (CNRS-INSU), contract no. 89-3620.

Appendix. R.m.s. turbulent velocity profiles of the velocity component parallel to the rotation axis

Hopfinger *et al.* (1983) measured the r.m.s. turbulent velocity component perpendicular to the rotation axis, but were not able to obtain the r.m.s. turbulent velocity component parallel to the rotation axis. The variation of the latter quantity along the direction of the rotation axis provides important information about the degree of two-dimensionality of the turbulence. The r.m.s. velocity component parallel to the rotation axis was measured during the course of this study using a laser-Doppler anemometer kindly placed at our disposal by TSI.

The variation of the r.m.s. turbulent velocity component parallel to the rotation axis is shown in figure 16. It is seen that, in the part of the tank nearest to the grid ($z < Z_T$), the horizontal and vertical turbulent velocity components decay in a similar manner, as they would decay in the absence of rotation. The vertical component is apparently smaller than the horizontal, but the difference is within experimental error, because the horizontal components (taken from Hopfinger *et al.* 1983) were not measured during the same experiment. In the upper part of the tank, where the decay of the horizontal component u ceases, the vertical component w decreases according to a linear law. For the conditions of figure 16, the mean rate of stretching, $|\partial w/\partial z| \approx 1.5 \times 10^{-2}$ s^{-1}, is much smaller than the x- or y-derivatives of the horizontal component $u/l \approx 2\Omega Ro \approx 1.2$ s^{-1}. For consistency with continuity, this property must be satisfied if the flow in a plane perpendicular to the rotation axis is in geostrophic equilibrium: $fu \approx -1/\rho\,\partial p/\partial y$ and $fv \approx 1/\rho\,\partial p/\partial x$ imply from the continuity equation that $\partial w/\partial z$ must be one order of magnitude smaller than $\partial u/\partial x$ and $\partial v/\partial y$. An additional proof that the turbulence in a plane perpendicular to the rotation axis is quasi-geostrophic is thus deduced from the profile of the r.m.s.

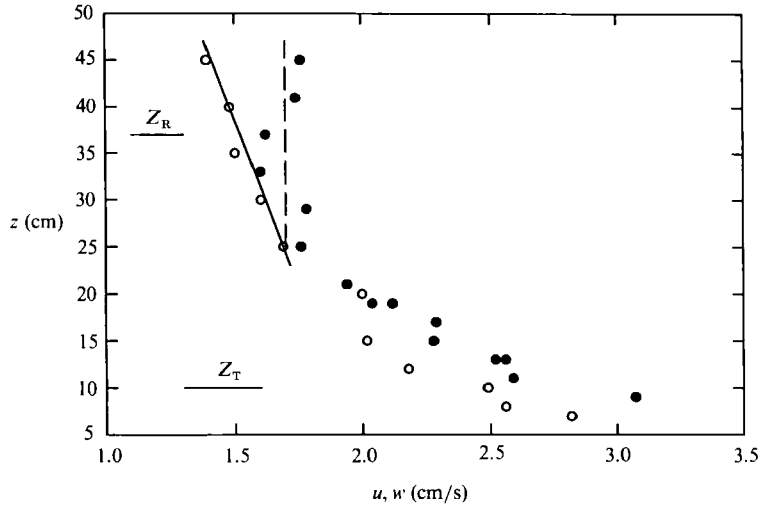

FIGURE 16. R.m.s. turbulent velocity components perpendicular (●) (measured by Hopfinger *et al.* 1983) and parallel (○) to the rotation axis of the tank, versus the distance from the grid midplane. Experimental conditions are $S = 4$ cm, $n = 6.6$ Hz, $\Omega = \pi$ rad s^{-1}.

velocity component parallel to the rotation axis. We also observe in figure 16 that the two velocity components are of the same order of magnitude. The pressure distribution is therefore not hydrostatic inside our tank as the lengthscale H parallel to the rotation axis is much larger than the lengthscale perpendicular to the rotation axis l. This is a major difference between the flow observed in our experiment and geophysical flows.

REFERENCES

BANK 1965 *Tables of Velocity of Sound*. Arthaud.

E, X. & HOPFINGER, E. J. 1986 On mixing across an interface in stably stratified fluid. *J. Fluid Mech.* **166**, 227–244.

FERNANDO, H. J. S. & LONG, R. R. 1985 On the nature of the entrainment interface of a two-layer fluid subjected to zero-mean-shear turbulence. *J. Fluid Mech.* **151**, 21–53.

FLEURY, M. 1988 Transferts turbulents à travers une interface de densité en milieu tournant. Thesis, Université J. Fourier, Grenoble.

HANNOUN, I. A., FERNANDO, H. J. S. & LIST, E. J. 1988 Turbulence structure near a sharp density interface. *J. Fluid Mech.* **189**, 189–209.

HANNOUN, I. A. & LIST, E. J. 1988 Turbulent mixing at a shear-free density interface. *J. Fluid Mech.* **189**, 211–234.

HOPFINGER, E. J., BROWAND, F. K. & GAGNE, Y. 1982 Turbulence and waves in a rotating tank. *J. Fluid Mech.* **125**, 505–534.

HOPFINGER, E. J., GRIFFITHS, R. W. & MORY, M. 1983 The structure of turbulence in homogeneous and stratified rotating fluid. *J. Méc. Theor. Appl. Special Issue*, pp. 21–44.

HOPFINGER, E. J. & TOLY, J. A. 1976 Spatially decaying turbulence and its relation to mixing across density interfaces. *J. Fluid Mech.* **78**, 155–175.

LINDEN, P. F. 1973 The interaction of a vortex ring with a sharp density interface: a model for turbulent entrainment. *J. Fluid Mech.* **60**, 467–480.

LONG, R. R. 1978 A theory of mixing in a stably stratified fluid. *J. Fluid Mech.* **84**, 113–124.

MCDOUGALL, T. J. 1979 Measurements of turbulence in a zero-mean shear mixed layer. *J. Fluid Mech.* **94**, 409–431.

MAXWORTHY, T. 1986 On turbulent mixing across a density interface in the presence of rotation. *J. Phys. Oceanogr.* **16**, 1136–1137.

MORY, M. 1991 A model of turbulent mixing across a density interface including the effect of rotation. *J. Fluid Mech.* **223**, 193–207.

MORY, M. & HOPFINGER, E. J. 1985 Rotating turbulence evolving freely from an initial quasi-2D state. Lecture Notes in Physics, vol. 230, Springer.

MORY, M. & HOPFINGER, E. J. 1986 Structure functions in a rotationally dominated turbulent flow. *Phys. Fluids* **29**, 2140–2146.

NOH, Y. & LONG, R. R. 1987 Turbulent mixing in a rotating fluid. *3rd Intl Symp. on Stratified Flows, Pasadena.*

NOKES, R. I. 1988 On the entrainment rate across a density interface. *J. Fluid Mech.* **188**, 188–204.

PHILLIPS, O. M. 1977 *Dynamics of the Upper Ocean.* Cambridge University Press.

THOMPSON, S. M. & TURNER, J. S. 1975 Mixing across an interface due to turbulence generated by an oscillating grid. *J. Fluid Mech.* **67**, 349–368.

TURNER, J. S. 1973 *Buoyancy Effects in Fluids.* Cambridge University Press.